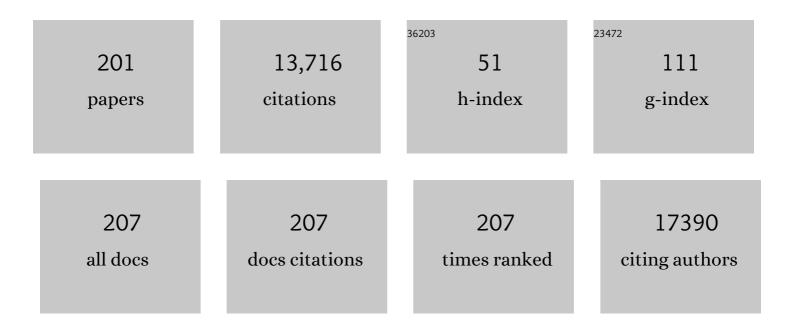
Dimosthenis Sokaras

List of Publications by Year in descending order

Source: https://exaly.com/author-pdf/1493524/publications.pdf Version: 2024-02-01



#	Article	IF	CITATIONS
1	Identification of Highly Active Fe Sites in (Ni,Fe)OOH for Electrocatalytic Water Splitting. Journal of the American Chemical Society, 2015, 137, 1305-1313.	6.6	2,018
2	Janus monolayers of transition metal dichalcogenides. Nature Nanotechnology, 2017, 12, 744-749.	15.6	1,459
3	Structures of the intermediates of Kok's photosynthetic water oxidation clock. Nature, 2018, 563, 421-425.	13.7	386
4	Tracking excited-state charge and spin dynamics in iron coordination complexes. Nature, 2014, 509, 345-348.	13.7	382
5	Simultaneous Femtosecond X-ray Spectroscopy and Diffraction of Photosystem II at Room Temperature. Science, 2013, 340, 491-495.	6.0	378
6	Structure of photosystem II and substrate binding at room temperature. Nature, 2016, 540, 453-457.	13.7	323
7	Designing Boron Nitride Islands in Carbon Materials for Efficient Electrochemical Synthesis of Hydrogen Peroxide. Journal of the American Chemical Society, 2018, 140, 7851-7859.	6.6	310
8	Targeted Ligand-Exchange Chemistry on Cesium Lead Halide Perovskite Quantum Dots for High-Efficiency Photovoltaics. Journal of the American Chemical Society, 2018, 140, 10504-10513.	6.6	303
9	Oxygen Release Induced Chemomechanical Breakdown of Layered Cathode Materials. Nano Letters, 2018, 18, 3241-3249.	4.5	237
10	Defective Carbon-Based Materials for the Electrochemical Synthesis of Hydrogen Peroxide. ACS Sustainable Chemistry and Engineering, 2018, 6, 311-317.	3.2	236
11	Identification of the active complex for CO oxidation over single-atom Ir-on-MgAl2O4 catalysts. Nature Catalysis, 2019, 2, 149-156.	16.1	222
12	Taking snapshots of photosynthetic water oxidation using femtosecond X-ray diffraction and spectroscopy. Nature Communications, 2014, 5, 4371.	5.8	206
13	Understanding Interactions between Manganese Oxide and Gold That Lead to Enhanced Activity for Electrocatalytic Water Oxidation. Journal of the American Chemical Society, 2014, 136, 4920-4926.	6.6	205
14	Phase segregation reversibility in mixed-metal hydroxide water oxidation catalysts. Nature Catalysis, 2020, 3, 743-753.	16.1	199
15	Nanoflow electrospinning serial femtosecond crystallography. Acta Crystallographica Section D: Biological Crystallography, 2012, 68, 1584-1587.	2.5	167
16	Fully Oxidized Ni–Fe Layered Double Hydroxide with 100% Exposed Active Sites for Catalyzing Oxygen Evolution Reaction. ACS Catalysis, 2019, 9, 6027-6032.	5.5	165
17	Systematic Structure–Property Relationship Studies in Palladium-Catalyzed Methane Complete Combustion. ACS Catalysis, 2017, 7, 7810-7821.	5.5	151
18	Drop-on-demand sample delivery for studying biocatalysts in action at X-ray free-electron lasers. Nature Methods, 2017, 14, 443-449.	9.0	150

#	Article	IF	CITATIONS
19	Room temperature femtosecond X-ray diffraction of photosystem II microcrystals. Proceedings of the National Academy of Sciences of the United States of America, 2012, 109, 9721-9726.	3.3	144
20	Accurate macromolecular structures using minimal measurements from X-ray free-electron lasers. Nature Methods, 2014, 11, 545-548.	9.0	140
21	Phase Transformation and Lithiation Effect on Electronic Structure of Li _{<i>x</i>} FePO ₄ : An In-Depth Study by Soft X-ray and Simulations. Journal of the American Chemical Society, 2012, 134, 13708-13715.	6.6	136
22	Extremely reduced dielectric confinement in two-dimensional hybrid perovskites with large polar organics. Communications Physics, 2018, 1, .	2.0	135
23	A seven-crystal Johann-type hard x-ray spectrometer at the Stanford Synchrotron Radiation Lightsource. Review of Scientific Instruments, 2013, 84, 053102.	0.6	132
24	A multi-crystal wavelength dispersive x-ray spectrometer. Review of Scientific Instruments, 2012, 83, 073114.	0.6	130
25	Depth-Dependent Redox Behavior of LiNi _{0.6} Mn _{0.2} Co _{0.2} O ₂ . Journal of the Electrochemical Society, 2018, 165, A696-A704.	1.3	123
26	Tunable metal hydroxide–organic frameworks for catalysing oxygen evolution. Nature Materials, 2022, 21, 673-680.	13.3	123
27	Effects of Gold Substrates on the Intrinsic and Extrinsic Activity of High-Loading Nickel-Based Oxyhydroxide Oxygen Evolution Catalysts. ACS Catalysis, 2017, 7, 5399-5409.	5.5	120
28	Energy-dispersive X-ray emission spectroscopy using an X-ray free-electron laser in a shot-by-shot mode. Proceedings of the National Academy of Sciences of the United States of America, 2012, 109, 19103-19107.	3.3	113
29	Acidic Oxygen Evolution Reaction Activity–Stability Relationships in Ru-Based Pyrochlores. ACS Catalysis, 2020, 10, 12182-12196.	5.5	111
30	Indications of radiation damage in ferredoxin microcrystals using high-intensity X-FEL beams. Journal of Synchrotron Radiation, 2015, 22, 225-238.	1.0	110
31	Metalloprotein entatic control of ligand-metal bonds quantified by ultrafast x-ray spectroscopy. Science, 2017, 356, 1276-1280.	6.0	109
32	Revealing and suppressing surface Mn(II) formation of Na0.44MnO2 electrodes for Na-ion batteries. Nano Energy, 2015, 16, 186-195.	8.2	107
33	An Oxygenâ€Insensitive Hydrogen Evolution Catalyst Coated by a Molybdenumâ€Based Layer for Overall Water Splitting. Angewandte Chemie - International Edition, 2017, 56, 5780-5784.	7.2	106
34	Electrochemical Oxidation of Size-Selected Pt Nanoparticles Studied Using in Situ High-Energy-Resolution X-ray Absorption Spectroscopy. ACS Catalysis, 2012, 2, 2371-2376.	5.5	105
35	Manipulating charge transfer excited state relaxation and spin crossover in iron coordination complexes with ligand substitution. Chemical Science, 2017, 8, 515-523.	3.7	102
36	Multiconfigurational nature of 5f orbitals in uranium and plutonium intermetallics. Proceedings of the National Academy of Sciences of the United States of America, 2012, 109, 10205-10209.	3.3	94

#	Article	IF	CITATIONS
37	Finding intersections between electronic excited state potential energy surfaces with simultaneous ultrafast X-ray scattering and spectroscopy. Chemical Science, 2019, 10, 5749-5760.	3.7	90
38	On the chemical state of Co oxide electrocatalysts during alkaline water splitting. Physical Chemistry Chemical Physics, 2013, 15, 17460. Femtosecond X-Ray Scattering, Study of Ultrafast Photoinduced Structural Dynamics in	1.3	89
39	Solvated <mml:math <br="" xmlns:mml="http://www.w3.org/1998/Math/MathML">display="inline"><mml:mrow><mml:mo stretchy="false">[</mml:mo><mml:mi>Co</mml:mi><mml:mo stretchy="false">(</mml:mo </mml:mrow></mml:math>		

DIMOSTHENIS SOKARAS

#	Article	IF	CITATIONS
55	Ultrafast terahertz field control of electronic and structural interactions in vanadium dioxide. Physical Review B, 2018, 98, .	1.1	49
56	Stimulated X-Ray Emission Spectroscopy in Transition Metal Complexes. Physical Review Letters, 2018, 120, 133203.	2.9	48
57	Combined elemental analysis of ancient glass beads by means of ion beam, portable XRF, and EPMA techniques. Analytical and Bioanalytical Chemistry, 2009, 395, 2199-2209.	1.9	47
58	Synchrotron imaging reveals bone healing and remodelling strategies in extinct and extant vertebrates. Journal of the Royal Society Interface, 2014, 11, 20140277.	1.5	47
59	Localized Electronic Structure of Nitrogenase FeMoco Revealed by Selenium K-Edge High Resolution X-ray Absorption Spectroscopy. Journal of the American Chemical Society, 2019, 141, 13676-13688.	6.6	47
60	Revealing Electronic Signatures of Lattice Oxygen Redox in Lithium Ruthenates and Implications for High-Energy Li-Ion Battery Material Designs. Chemistry of Materials, 2019, 31, 7864-7876.	3.2	47
61	Simultaneous detection of electronic structure changes from two elements of a bifunctional catalyst using wavelength-dispersive X-ray emission spectroscopy and in situ electrochemistry. Physical Chemistry Chemical Physics, 2015, 17, 8901-8912.	1.3	45
62	Empowering multicomponent cathode materials for sodium ion batteries by exploring three-dimensional compositional heterogeneities. Energy and Environmental Science, 2018, 11, 2496-2508.	15.6	45
63	Thermal stress-induced charge and structure heterogeneity in emerging cathode materials. Materials Today, 2020, 35, 87-98.	8.3	45
64	X-ray Fluorescence analytical criteria to assess the fineness of ancient silver coins: Application on Ptolemaic coinage. Spectrochimica Acta, Part B: Atomic Spectroscopy, 2011, 66, 681-690.	1.5	44
65	Elemental characterisation of melanin in feathers via synchrotron X-ray imaging and absorption spectroscopy. Scientific Reports, 2016, 6, 34002.	1.6	44
66	Finite temperature effects on the X-ray absorption spectra of lithium compounds: First-principles interpretation of X-ray Raman measurements. Journal of Chemical Physics, 2014, 140, 034107.	1.2	43
67	Oxidation and crystal field effects in uranium. Physical Review B, 2015, 92, .	1.1	43
68	Direct Observation of Methylmercury and Auranofin Binding to Selenocysteine in Thioredoxin Reductase. Inorganic Chemistry, 2020, 59, 2711-2718.	1.9	43
69	Ligand manipulation of charge transfer excited state relaxation and spin crossover in [Fe(2,2′-bipyridine)2(CN)2]. Structural Dynamics, 2017, 4, 044030.	0.9	41
70	Hot Branching Dynamics in a Lightâ€Harvesting Iron Carbene Complex Revealed by Ultrafast Xâ€ray Emission Spectroscopy. Angewandte Chemie - International Edition, 2020, 59, 364-372.	7.2	41
71	Unveiling the critical role of the Mn dopant in a NiFe(OH) ₂ catalyst for water oxidation. Journal of Materials Chemistry A, 2020, 8, 17471-17476.	5.2	41
72	Towards controlling the reversibility of anionic redox in transition metal oxides for high-energy Li-ion positive electrodes. Energy and Environmental Science, 2021, 14, 2322-2334.	15.6	41

#	Article	IF	CITATIONS
73	Soft X-ray spectroscopy with transition-edge sensors at Stanford Synchrotron Radiation Lightsource beamline 10-1. Review of Scientific Instruments, 2019, 90, 113101.	0.6	40
74	Rethinking the Minamata Tragedy: What Mercury Species Was Really Responsible?. Environmental Science & Technology, 2020, 54, 2726-2733.	4.6	40
75	Structural changes correlated with magnetic spin state isomorphism in the S ₂ state of the Mn ₄ CaO ₅ cluster in the oxygen-evolving complex of photosystem II. Chemical Science, 2016, 7, 5236-5248.	3.7	39
76	Operando investigation of Au-MnOx thin films with improved activity for the oxygen evolution reaction. Electrochimica Acta, 2017, 230, 22-28.	2.6	39
77	X-ray Emission Spectroscopy as an <i>in Situ</i> Diagnostic Tool for X-ray Crystallography of Metalloproteins Using an X-ray Free-Electron Laser. Biochemistry, 2018, 57, 4629-4637.	1.2	39
78	Delocalization and occupancy effects of 5f orbitals in plutonium intermetallics using L3-edge resonant X-ray emission spectroscopy. Journal of Electron Spectroscopy and Related Phenomena, 2014, 194, 57-65.	0.8	37
79	Leaf metallome preserved over 50 million years. Metallomics, 2014, 6, 774-782.	1.0	35
80	Self-Doping and Electrical Conductivity in Spinel Oxides: Experimental Validation of Doping Rules. Chemistry of Materials, 2014, 26, 1867-1873.	3.2	35
81	Photon-in photon-out hard X-ray spectroscopy at the Linac Coherent Light Source. Journal of Synchrotron Radiation, 2015, 22, 612-620.	1.0	35
82	Highâ€Energyâ€Resolution Xâ€ray Absorption Spectroscopy for Identification of Reactive Surface Species on Supported Singleâ€Site Iridium Catalysts. Chemistry - A European Journal, 2017, 23, 14760-14768.	1.7	35
83	Operando Study of Thermal Oxidation of Monolayer MoS ₂ . Advanced Science, 2021, 8, 2002768.	5.6	35
84	Performance of a polycapillary halflens as focussing and collecting optic—a comparison. Journal of Analytical Atomic Spectrometry, 2009, 24, 669.	1.6	32
85	3D Micro PIXE—a new technique for depth-resolved elemental analysis. Journal of Analytical Atomic Spectrometry, 2007, 22, 1260.	1.6	31
86	Kβ Valence to Core X-ray Emission Studies of Cu(I) Binding Proteins with Mixed Methionine – Histidine Coordination. Relevance to the Reactivity of the M- and H-sites of Peptidylglycine Monooxygenase. Inorganic Chemistry, 2016, 55, 3431-3439.	1.9	30
87	Pheomelanin pigment remnants mapped in fossils of an extinct mammal. Nature Communications, 2019, 10, 2250.	5.8	30
88	X-ray Absorption Spectroscopy Investigations of Copper(II) Coordination in the Human Amyloid \hat{I}^2 Peptide. Inorganic Chemistry, 2019, 58, 6294-6311.	1.9	30
89	Charge and Spin-State Characterization of Cobalt Bis(<i>o</i> -dioxolene) Valence Tautomers Using Co Kî² X-ray Emission and L-Edge X-ray Absorption Spectroscopies. Inorganic Chemistry, 2017, 56, 737-747.	1.9	29
90	In situ X-ray Raman spectroscopy study of the hydrogen sorption properties of lithium borohydride nanocomposites. Physical Chemistry Chemical Physics, 2014, 16, 22651-22658.	1.3	28

#	Article	IF	CITATIONS
91	The mapping and differentiation of biological and environmental elemental signatures in the fossil remains of a 50 million year old bird. Journal of Analytical Atomic Spectrometry, 2015, 30, 627-634.	1.6	28
92	Ultrafast nonthermal heating of water initiated by an X-ray Free-Electron Laser. Proceedings of the National Academy of Sciences of the United States of America, 2018, 115, 5652-5657.	3.3	28
93	Resonant inelastic X-ray scattering determination of the electronic structure of oxyhemoglobin and its model complex. Proceedings of the National Academy of Sciences of the United States of America, 2019, 116, 2854-2859.	3.3	28
94	Mechanistic and Electronic Insights into a Working NiAu Single-Atom Alloy Ethanol Dehydrogenation Catalyst. Journal of the American Chemical Society, 2021, 143, 21567-21579.	6.6	28
95	In situ X-ray Raman spectroscopy of LiBH4. Physical Chemistry Chemical Physics, 2012, 14, 5581.	1.3	27
96	Geometry of electromechanically active structures in Gadolinium - doped Cerium oxides. AIP Advances, 2016, 6, 055320.	0.6	27
97	Noninvasive Synchrotron-Based X-ray Raman Scattering Discriminates Carbonaceous Compounds in Ancient and Historical Materials. Analytical Chemistry, 2017, 89, 10819-10826.	3.2	27
98	Operando Elucidation on the Working State of Immobilized Fluorinated Iron Porphyrin for Selective Aqueous Electroreduction of CO ₂ to CO. ACS Catalysis, 2021, 11, 6499-6509.	5.5	27
99	A versatile Johansson-type tender x-ray emission spectrometer. Review of Scientific Instruments, 2020, 91, 033101.	0.6	26
100	Hard X-rays in–soft X-rays out: An operando piggyback view deep into a charging lithium ion battery with X-ray Raman spectroscopy. Journal of Electron Spectroscopy and Related Phenomena, 2015, 200, 257-263	0.8	25
101	xmlns:mml="http://www.w3.org/1998/Math/MathML"> <mml:mrow><mml:mn>5</mml:mn> <mml:mi>f</mml:mi> configurations in<mml:math xmlns:mml="http://www.w3.org/1998/Math/MathML"><mml:mrow><mml:msub><mml:mi>URu</mml:mi><mml:n U<mml:math< td=""><td></td><td></td></mml:math<></mml:n </mml:msub></mml:mrow></mml:math </mml:mrow>		
102	To Transfer or Not to Transfer? Development of a Dinitrosyl Iron Complex as a Nitroxyl Donor for the Nitroxylation of an Fe ^{III} –Porphyrin Center. Chemistry - A European Journal, 2015, 21, 17570-17573.	itext>1.7	ml:msub> <br 24
103	L-edge spectroscopy of dilute, radiation-sensitive systems using a transition-edge-sensor array. Journal of Chemical Physics, 2017, 147, 214201.	1.2	24
104	Secondary Fluorescence Enhancement in Confocal X-ray Microscopy Analysis. Analytical Chemistry, 2009, 81, 4946-4954.	3.2	23
105	Determining Atomic-Scale Structure and Composition of Organo-Lead Halide Perovskites by Combining High-Resolution X-ray Absorption Spectroscopy and First-Principles Calculations. ACS Energy Letters, 2017, 2, 1183-1189.	8.8	23
106	Electronic structure changes upon lithium intercalation into graphite – Insights from ex situ and operando x-ray Raman spectroscopy. Carbon, 2019, 143, 371-377.	5.4	22
107	3D Micro-PIXE at atmospheric pressure: A new tool for the investigation of art and archaeological objects. Nuclear Instruments & Methods in Physics Research B, 2007, 264, 383-388.	0.6	21
108	New insights into the chemical and isotopic composition of human-body biominerals. I: Cholesterol gallstones from England and Greece. Journal of Trace Elements in Medicine and Biology, 2013, 27, 79-84.	1.5	21

DIMOSTHENIS SOKARAS

#	Article	IF	CITATIONS
109	Covalency in oxidized uranium. Physical Review B, 2015, 92, .	1.1	21
110	Resolving structures of transition metal complex reaction intermediates with femtosecond EXAFS. Physical Chemistry Chemical Physics, 2020, 22, 2660-2666.	1.3	21
111	Manipulating electron redistribution to achieve electronic pyroelectricity in molecular [FeCo] crystals. Nature Communications, 2021, 12, 4836.	5.8	21
112	[Ni ^{III} (OMe)]-mediated reductive activation of CO ₂ affording a Ni(κ ¹ -OCO) complex. Chemical Science, 2016, 7, 3640-3644.	3.7	20
113	Observation of Seeded Mn Kβ Stimulated X-Ray Emission Using Two-Color X-Ray Free-Electron Laser Pulses. Physical Review Letters, 2020, 125, 037404.	2.9	20
114	In situ X-ray diffraction of silicate liquids and glasses under dynamic and static compression to megabar pressures. Proceedings of the National Academy of Sciences of the United States of America, 2020, 117, 11981-11986.	3.3	20
115	Solvation structures of protons and hydroxide ions in water. Journal of Chemical Physics, 2013, 138, 154506.	1.2	19
116	Towards characterization of photo-excited electron transfer and catalysis in natural and artificial systems using XFELs. Faraday Discussions, 2016, 194, 621-638.	1.6	19
117	Separate measurement of the 5f5/2 and 5f7/2 unoccupied density of states of UO2. Journal of Electron Spectroscopy and Related Phenomena, 2019, 232, 100-104.	0.8	19
118	EXAFS as a probe of actinide oxide formation in the tender X-ray regime. Surface Science, 2020, 698, 121607.	0.8	19
119	Distinct Surface and Bulk Thermal Behaviors of LiNi _{0.6} Mn _{0.2} Co _{0.2} O ₂ Cathode Materials as a Function of State of Charge. ACS Applied Materials & Interfaces, 2020, 12, 11643-11656.	4.0	19
120	Observation of 5f intermediate coupling in uranium x-ray emission spectroscopy. Journal of Physics Communications, 2020, 4, 015013.	0.5	19
121	Focus characterization at an X-ray free-electron laser by coherent scattering and speckle analysis. Journal of Synchrotron Radiation, 2015, 22, 599-605.	1.0	18
122	Operando Observation of Chemical Transformations of Iridium Oxide During Photoelectrochemical Water Oxidation. ACS Applied Energy Materials, 2019, 2, 1371-1379.	2.5	18
123	Sulfur Kβ X-ray emission spectroscopy: comparison with sulfur K-edge X-ray absorption spectroscopy for speciation of organosulfur compounds. Physical Chemistry Chemical Physics, 2021, 23, 4500-4508.	1.3	18
124	Electronic structure study of the CdS buffer layer in CIGS solar cells by X-ray absorption spectroscopy: Experiment and theory. Solar Energy Materials and Solar Cells, 2016, 149, 275-283.	3.0	17
125	Application of FEFF analyses to actinide 5f systems. Journal of Vacuum Science and Technology A: Vacuum, Surfaces and Films, 2020, 38, .	0.9	17
126	Calcium-Uranyl-Carbonato Species Kinetically Limit U(VI) Reduction by Fe(II) and Lead to U(V)-Bearing Ferrihydrite. Environmental Science & Technology, 2020, 54, 6021-6030.	4.6	17

#	Article	IF	CITATIONS
127	Short-lived metal-centered excited state initiates iron-methionine photodissociation in ferrous cytochrome c. Nature Communications, 2021, 12, 1086.	5.8	17
128	Revealing the bonding of solvated Ru complexes with valence-to-core resonant inelastic X-ray scattering. Chemical Science, 2021, 12, 3713-3725.	3.7	17
129	Characterization of a Dynamic Y ₂ Ir ₂ O ₇ Catalyst during the Oxygen Evolution Reaction in Acid. Journal of Physical Chemistry C, 2022, 126, 1751-1760.	1.5	17
130	Local Structure of Sulfur Vacancies on the Basal Plane of Monolayer MoS ₂ . ACS Nano, 2022, 16, 6725-6733.	7.3	17
131	Three-dimensional imaging of aerosol particles with scanning proton microprobe in a confocal arrangement. Applied Physics Letters, 2008, 93, 094104. Cascade <mml:math <="" td="" xmlns:mml="http://www.w3.org/1998/Math/MathML"><td>1.5</td><td>16</td></mml:math>	1.5	16
132	display="inline"> <mml:mrow> <mml:mi>L</mml:mi>K</mml:mrow> -shell soft-x-ray emission as incident x-ray photons are tuned across the <mml:math xmlns:mml="http://www.w3.org/1998/Math/MathML" display="inline"><mml:mrow> <mml:mn> 1</mml:mn> </mml:mrow> ionization</mml:math 	1.0	16
133	threshold. Physical Review A, 2011, 83, . Using N-Terminal Coordination of Cu(II) and Ni(II) to Isolate the Coordination Environment of Cu(I) and Cu(II) Bound to His13 and His14 in Amyloid-I²(4–16). Inorganic Chemistry, 2019, 58, 15138-15154.	1.9	16
134	Resonant Inelastic X-ray Scattering Calculations of Transition Metal Complexes Within a Simplified Time-Dependent Density Functional Theory Framework. Journal of Chemical Theory and Computation, 2021, 17, 3031-3038.	2.3	16
135	Referenceâ€free xâ€ray fluorescence analysis of an ancient Chinese ceramic. X-Ray Spectrometry, 2008, 37, 462-465.	0.9	15
136	Quantitative analysis in confocal micro-PIXE—general concept and layered materials. Journal of Analytical Atomic Spectrometry, 2009, 24, 611.	1.6	15
137	The new external ion beam analysis setup at the Demokritos Tandem accelerator and first applications in cultural heritage. Nuclear Instruments & Methods in Physics Research B, 2011, 269, 519-527.	0.6	15
138	Excited state charge distribution and bond expansion of ferrous complexes observed with femtosecond valence-to-core x-ray emission spectroscopy. Journal of Chemical Physics, 2020, 152, 074203.	1.2	15
139	Bioturbating animals control the mobility of redox-sensitive trace elements in organic-rich mudstone. Geology, 2015, 43, 1007-1010.	2.0	14
140	A Photochemically Generated Selenyl Free Radical Observed by High Energy Resolution Fluorescence Detected X-ray Absorption Spectroscopy. Inorganic Chemistry, 2018, 57, 10867-10872.	1.9	14
141	Hot Branching Dynamics in a Lightâ€Harvesting Iron Carbene Complex Revealed by Ultrafast Xâ€ray Emission Spectroscopy. Angewandte Chemie, 2020, 132, 372-380.	1.6	14
142	Probing Depth-Dependent Transition-Metal Redox of Lithium Nickel, Manganese, and Cobalt Oxides in Li-Ion Batteries. ACS Applied Materials & Interfaces, 2020, 12, 55865-55875.	4.0	14
143	High Energy Resolution Fluorescence Detected X-ray Absorption Spectroscopy: An Analytical Method for Selenium Speciation. Analytical Chemistry, 2021, 93, 9235-9243.	3.2	14
144	Base-Accelerated Degradation of Nanosized Platinum Electrocatalysts. ACS Catalysis, 2021, 11, 9904-9915.	5.5	14

#	Article	IF	CITATIONS
145	Resonant Raman scattering of polarized and unpolarized x-ray radiation from Mg, Al, and Si. Physical Review A, 2010, 81, .	1.0	13
146	Surface Characterization of Li-Substituted Compositionally Heterogeneous NaLi _{0.045} Cu _{0.185} Fe _{0.265} Mn _{0.505} O ₂ Sodium-Ion Cathode Material. Journal of Physical Chemistry C, 2019, 123, 11428-11435.	1.5	13
147	Femtosecond electronic structure response to high intensity XFEL pulses probed by iron X-ray emission spectroscopy. Scientific Reports, 2020, 10, 16837.	1.6	13
148	On the valence fluctuation in the early actinide metals. Journal of Electron Spectroscopy and Related Phenomena, 2016, 207, 14-18.	0.8	12
149	Electronic structure studies reveal 4f/5d mixing and its effect on bonding characteristics in Ce-imido and -oxo complexes. Chemical Science, 2022, 13, 1759-1773.	3.7	12
150	Molecular Fates of Organometallic Mercury in Human Brain. ACS Chemical Neuroscience, 2022, 13, 1756-1768.	1.7	12
151	Carbon Core Electron Spectra of Polycyclic Aromatic Hydrocarbons. Journal of Physical Chemistry A, 2018, 122, 5730-5734.	1.1	11
152	Quantifying the Application of FEFF to f-derived Spectral Structure. MRS Advances, 2020, 5, 2631-2638.	0.5	11
153	Towards the Quantification of 5f Delocalization. Applied Sciences (Switzerland), 2020, 10, 2918.	1.3	11
154	A high-throughput energy-dispersive tender X-ray spectrometer for shot-to-shot sulfur measurements. Journal of Synchrotron Radiation, 2019, 26, 629-634.	1.0	11
155	In situ scanning micro-XRF analyses of gilded bronze figurines at the National Museum of Damascus. Journal of Analytical Atomic Spectrometry, 2015, 30, 1787-1798.	1.6	10
156	Effect of 3d/4p Mixing on 1s2p Resonant Inelastic X-ray Scattering: Electronic Structure of Oxo-Bridged Iron Dimers. Journal of the American Chemical Society, 2021, 143, 4569-4584.	6.6	10
157	Kβ X-ray Emission Spectroscopy as a Probe of Cu(I) Sites: Application to the Cu(I) Site in Preprocessed Galactose Oxidase. Inorganic Chemistry, 2020, 59, 16567-16581.	1.9	10
158	Effects of x-ray free-electron laser pulse intensity on the Mn K <i>β</i> _{1,3} x-ray emission spectrum in photosystem II—A case study for metalloprotein crystals and solutions. Structural Dynamics, 2021, 8, 064302.	0.9	10
159	Two-photon absorption of soft X-ray free electron laser radiation by graphite near the carbon K-absorption edge. Chemical Physics Letters, 2018, 703, 112-116.	1.2	9
160	Hybrid X-ray Spectroscopy-Based Approach To Acquire Chemical and Structural Information of Single-Walled Carbon Nanotubes with Superior Sensitivity. Journal of Physical Chemistry C, 2019, 123, 6114-6120.	1.5	9
161	Femtosecond X-ray Spectroscopy Directly Quantifies Transient Excited-State Mixed Valency. Journal of Physical Chemistry Letters, 2022, 13, 378-386.	2.1	9
162	Unoccupied electronic structure of actinide dioxides. Physical Review B, 2022, 105, .	1.1	9

DIMOSTHENIS SOKARAS

#	Article	IF	CITATIONS
163	Local vs Nonlocal States in FeTiO ₃ Probed with 1s2pRIXS: Implications for Photochemistry. Inorganic Chemistry, 2017, 56, 10882-10892.	1.9	8
164	Probing U 5f Covalency in Uranium Compounds through Oxidant 2p Bonding. Journal of the Physical Society of Japan, 2020, 89, 024711.	0.7	8
165	The X-ray emission of cerium oxide. Journal of Electron Spectroscopy and Related Phenomena, 2021, 246, 147007.	0.8	8
166	Elementâ€selective threeâ€dimensional imaging of microparticles with a confocal microâ€PIXE arrangement. X-Ray Spectrometry, 2009, 38, 526-539.	0.9	7
167	3D-reconstruction of an object by means of a confocal micro-PIXE. Journal of Analytical Atomic Spectrometry, 2010, 25, 28-33.	1.6	7
168	Hg(II) Binding to Thymine Bases in DNA. Inorganic Chemistry, 2021, 60, 7442-7452.	1.9	7
169	Underlying simplicity of 5f unoccupied electronic structure. Journal of Vacuum Science and Technology A: Vacuum, Surfaces and Films, 2021, 39, .	0.9	7
170	Quantification of Ni–N–O Bond Angles and NO Activation by X-ray Emission Spectroscopy. Inorganic Chemistry, 2021, 60, 736-744.	1.9	7
171	Mercury Lα1 High Energy Resolution Fluorescence Detected X-ray Absorption Spectroscopy: A Versatile Speciation Probe for Mercury. Inorganic Chemistry, 2022, 61, 5201-5214.	1.9	7
172	Construction of a confocal PIXE set-up at the Jožef Stefan Institute and first results. Nuclear Instruments & Methods in Physics Research B, 2011, 269, 2237-2243.	0.6	6
173	Electronic Structure of Naturally Occurring Aromatic Carbon. Energy & amp; Fuels, 2019, 33, 2099-2105.	2.5	6
174	Diagram, valenceâ€toâ€core, and hypersatellite <i>Kβ</i> Xâ€ray transitions in metallic chromium. X-Ray Spectrometry, 2019, 48, 351-359.	0.9	6
175	Solution Chemistry of Copper(II) Binding to Substituted 8-Hydroxyquinolines. Inorganic Chemistry, 2020, 59, 13858-13874.	1.9	6
176	The Limitations of 5f Delocalization and Dispersion. Applied Sciences (Switzerland), 2021, 11, 3882.	1.3	6
177	High-resolution x-ray-emission study of < mml:math xmlns:mml="http://www.w3.org/1998/Math/MathML"> < mml:mrow> < mml:mn> 1 < /mml:mn> < mml:mi> s < /mml:m xmlns:mml="http://www.w3.org/1998/Math/MathML"> < mml:mrow> < mml:mn> 1 < /mml:mn> < mml:mi> s < /mml:m photoexcitations in Kr. Physical Review A. 2014. 90	i> <mml:m i> <mml:m< td=""><td>n>4n>3</td></mml:m<></mml:m 	n>4n>3
178	Reply to Comments on "Rethinking the Minamata Tragedy: What Mercury Species Was Really Responsible?― Environmental Science & Technology, 2020, 54, 8488-8490.	4.6	5
179	X-ray Raman Scattering: A Hard X-ray Probe of Complex Organic Systems. Chemical Reviews, 2022, 122, 12977-13005.	23.0	5
180	Proton induced quasi-monochromatic x-ray beams for soft x-ray spectroscopy studies and selective x-ray fluorescence analysis. Review of Scientific Instruments, 2012, 83, 123102.	0.6	4

#	Article	IF	CITATIONS
181	Morphological and chemical evidence for cyclic bone growth in a fossil hyaena. Journal of Analytical Atomic Spectrometry, 2018, 33, 2062-2069.	1.6	4
182	NpSe ₂ : a Binary Chalcogenide Containing Modulated Selenide Chains and Ambiguousâ€Valent Metal. Angewandte Chemie - International Edition, 2019, 58, 16130-16133.	7.2	4
183	Millisecond timescale reactions observed via X-ray spectroscopy in a 3D microfabricated fused silica mixer. Journal of Synchrotron Radiation, 2021, 28, 1100-1113.	1.0	4
184	Nature of cobalt species during the <i>in situ</i> sulfurization of Co(Ni)Mo/Al ₂ O ₃ hydrodesulfurization catalysts. Journal of Synchrotron Radiation, 2019, 26, 811-818.	1.0	4
185	Generation of intense phase-stable femtosecond hard X-ray pulse pairs. Proceedings of the National Academy of Sciences of the United States of America, 2022, 119, e2119616119.	3.3	4
186	Effect of doping TiO ₂ with Mn for electrocatalytic oxidation in acid and alkaline electrolytes. Energy Advances, 2022, 1, 357-366.	1.4	4
187	Disentangling the chemistry of Australian plant exudates from a unique historical collection. Proceedings of the National Academy of Sciences of the United States of America, 2022, 119, .	3.3	4
188	Visualizing sulfur with X-rays: From molecules to tissues. Phosphorus, Sulfur and Silicon and the Related Elements, 2019, 194, 618-623.	0.8	3
189	Reply to Comments on "Rethinking the Minamata Tragedy: What Mercury Species Was Really Responsible?― Environmental Science & Technology, 2020, 54, 8484-8485.	4.6	3
190	Comment on "Underlying simplicity of 5f unoccupied electronic structure―[J. Vac. Sci. Technol. A 39, 043205 (2021)]. Journal of Vacuum Science and Technology A: Vacuum, Surfaces and Films, 2021, 39, .	0.9	3
191	Determination of differential cross-sections for the natK(p,p0) and 39K(p,α0) reactions in the backscattering geometry. Nuclear Instruments & Methods in Physics Research B, 2010, 268, 1797-1801.	0.6	2
192	Probing Charge Ordering in Fractional Mixed-Valence Charge Density Wave Systems with Oriented HERFD-XANES Spectroscopy. Journal of Physical Chemistry C, 2020, 124, 16544-16552.	1.5	2
193	Chemically directing d-block heterometallics to nanocrystal surfaces as molecular beacons of surface structure. Chemical Science, 2015, 6, 6295-6304.	3.7	1
194	U M subshell X-ray emission spectroscopy of uranium dioxide: the effect of excitation energy. MRS Advances, 2021, 6, 209-212.	0.5	1
195	High Energy Resolution X-ray Spectroscopy at SSRL and LCLS: Instruments and Applications. Acta Crystallographica Section A: Foundations and Advances, 2014, 70, C223-C223.	0.0	Ο
196	Soft X-ray absorption spectroscopy investigation of the surface chemistry and treatments of copper indium gallium diselenide (CIGS). Solar Energy Materials and Solar Cells, 2017, 160, 390-397.	3.0	0
197	High Resolution, Seamless ePix10K Cameras for Wavelength-Dispersive Spectroscopy. , 2018, , .		0
198	Hammerhead, an ultrahigh resolution ePix camera for wavelength-dispersive spectrometers. AIP Conference Proceedings, 2019, , .	0.3	0

#	Article	IF	CITATIONS
199	Analytic von Hamos geometry optimization and calibration. , 2021, , .		Ο
200	F-39 <i>Invited</i> — Micro-XRF Analysis of Metal Alloys: From the Laboratory Calibration Towards In-Situ Analyses. Powder Diffraction, 2010, 25, 214-214.	0.4	0
201	Thorium model and weak 5f delocalization. Journal of Vacuum Science and Technology A: Vacuum, Surfaces and Films, 2022, 40, 033205.	0.9	0